Supplementary Material for
Mapping distinct timescales of functional interactions among brain networks

Mali Sundaresan
s.malisundar@gmail.com

Arshed Nabeel
arshed@iisc.ac.in

Devarajan Sridharan*
sridhar@iisc.ac.in

S1 Granger Causality estimation using MVAR modelling [5]

Consider the random vector $\mathbf{q}[t]$ whose time evolution is modeled by the following multivariate autoregressive model ("full" model):

$$\mathbf{q}[t] = \sum_{i=1}^{p} A_i \mathbf{q}[t-p] + \mathbf{e}[t] \tag{1}$$

Let $\mathbf{q} = [\mathbf{x}^\top \mathbf{y}^\top \mathbf{z}^\top]^\top$, where $\mathbf{x}, \mathbf{y}$ and $\mathbf{z}$ are themselves random vectors. $\mathbf{e}$ is the residual (prediction error) of the full model, with covariance T. T can be expressed as comprising the following block matrices:

$$T = \begin{bmatrix} T_{\mathbf{x}} & T_{\mathbf{xy}} & T_{\mathbf{xz}} \\ T_{\mathbf{xy}}^\top & T_{\mathbf{y}} & T_{\mathbf{yz}} \\ T_{\mathbf{xz}}^\top & T_{\mathbf{yz}}^\top & T_{\mathbf{z}} \end{bmatrix} \tag{2}$$

where the submatrices $T_{\mathbf{x}}, T_{\mathbf{y}}$ and $T_{\mathbf{z}}$ are the covariances of the residuals associated with $\mathbf{x}, \mathbf{y}$ and $\mathbf{z}$ (rows), respectively, and $T_{\mathbf{xy}}$ etc are the covariance between the residuals associated with $\mathbf{x}$ and $\mathbf{y}$, etc.

We define the following *reduced* vector autoregressive processes.

$$\mathbf{x}[t] = \sum_{i=1}^{p} A_i^{(\mathbf{xx})} \mathbf{x}[t-p] + \sum_{i=1}^{p} A_i^{(\mathbf{xz})} \mathbf{z}[t-p] + \mathbf{u}[t] \tag{3}$$

$$\mathbf{y}[t] = \sum_{i=1}^{p} A_i^{(\mathbf{yy})} \mathbf{y}[t-p] + \sum_{i=1}^{p} A_i^{(\mathbf{yz})} \mathbf{z}[t-p] + \mathbf{v}[t] \tag{4}$$

$$\tag{5}$$

$\mathbf{u}$ and $\mathbf{v}$ are the residuals of the reduced VAR models, with respective covariance matrices $S_{\mathbf{x}}$ and $S_{\mathbf{y}}$.

The conditional linear dependence between $\mathbf{x}$ and $\mathbf{y}$, conditioned on $\mathbf{z}$, is given by the following equations.

$$\mathcal{F}_{\mathbf{x}\to\mathbf{y}|\mathbf{z}} = \ln \frac{|S_{\mathbf{y}}|}{|T_{\mathbf{y}}|} \tag{6}$$

$$\mathcal{F}_{\mathbf{y}\to\mathbf{x}|\mathbf{z}} = \ln \frac{|S_{\mathbf{x}}|}{|T_{\mathbf{x}}|} \tag{7}$$

$$\mathcal{F}_{\mathbf{x}\circ\mathbf{y}|\mathbf{z}} = \ln \frac{|T_{\mathbf{x}}|\,|T_{\mathbf{y}}|}{|T'|} \tag{8}$$

$$\mathcal{F}_{\mathbf{x},\mathbf{y}|\mathbf{z}} = \mathcal{F}_{\mathbf{x}\to\mathbf{y}} + \mathcal{F}_{\mathbf{y}\to\mathbf{x}} + \mathcal{F}_{\mathbf{x}\circ\mathbf{y}} \tag{9}$$

$$= \ln \frac{|S_{\mathbf{x}}|\,|S_{\mathbf{y}}|}{|T'|} \tag{10}$$

*Corresponding author

31st Conference on Neural Information Processing Systems (NIPS 2017), Long Beach, CA, USA.

where $T' = \begin{bmatrix} T_{\mathbf{x}} & T_{\mathbf{xy}} \\ T_{\mathbf{xy}}^{\top} & T_{\mathbf{y}} \end{bmatrix}$

S2 Analytic computation of instantaneous correlations

We consider the case of a two node network and find the analytic solution of correlations between the node time series. The process is simulated as a linear dynamical system of the form:

$$\dot{\mathbf{x}} = A\mathbf{x} + \varepsilon$$

Assuming ε to be a zero mean Gaussian white noise process with covariance Q, it can be shown that the covariance X of time series $\mathbf{x}$ satisfies the Lyapunov equation:

$$AX + XA^T + Q = 0$$

Assuming $A = \begin{bmatrix} -1 & c \\ d & -1 \end{bmatrix}$, it can be shown that the covariance between the components of $\mathbf{x}$ ($X(1,2)$) is a non linear function of $c + d$ and has the same sign as $c + d$ (*lyap* function in Matlab). Importantly, the covariance (and correlation) is 0 for the case of reciprocal excitatory-inhibitory connectivity, for which $c = -d$. This is the reason why iGC and partial correlations, both of which rely on instantaneous correlations failed to capture reciprocal E-I interactions, as shown in Figure 2A (main text).

S3 fMRI data and time series extraction

We used minimally preprocessed data [6] provided by HCP Consortium[2], for our study. Supplementary Material Fig S8 shows the ids of the 500 subjects who were included in this analysis.

We used a functional 14-network or 90-regional parcellation[3]. Matlab and SPM8[4] were used to extract network time series data from preprocessed scans. The 14 functional networks included here are listed in table Supplementary Material Table S2, along with our abbreviated names for each. We adopted this parcellation, with fewer, more coarse-grained regions, rather than a finer parcellation (e.g. a 274 region functional parcellation [8]) because GC estimates were more reliable when the number of regions was far fewer than the number of timepoints. Both task and resting scans were of sufficient duration ($\sim$200-300 volumes) to permit robust GC estimation. In simulations, we noticed that the magnitude of GC estimates varied based on the number of timepoints used in the estimation. To prevent this difference in number of timepoints from biasing classification performance, we truncated each scan to a common minimum number of time samples for each task and resting scan before estimating GC. Finally, in this parcellation, there were overlapping voxels between some of the networks. To avoid mixing of signals, we assigned each overlapping voxel to the network whose centroid it was closest to.

S4 Permutation testing

We performed permutation tests for evaluating the statistical significance of classifier performance, using the method outlined in [7]. We conducted these for the language task versus resting state classification, separately for the three metrics (dGC, iGC and fGC).

The first test involved permuting task labels independently for each subject and computing a null distribution of leave-one-out accuracy. We employed 10000 surrogates and confirmed that each of the accuracy values for iGC, dGC and fGC based classifiers (reported in Fig. 3, main text) was significant ($p < 0.0001$).

The second test [7] measures how much of the classification performance is due simply to the differences in the correlation structure of the feature dimensions across resting and task. This was done by permuting the feature dimensions class-wise, and comparing the accuracy of the resultant

[2] http://www.humanconnectome.org/

[3] http://findlab.stanford.edu/functional_ROIs.html

[4] www.fil.ion.ucl.ac.uk/spm/software/spm8/

classification with the original classification accuracy. We observed that for dGC, RFE accuracy remained similar (80.6%) even after permutation, and over 80% of RFE features were preserved. On the other hand, for iGC, RFE accuracy reduced to 58.8% and only 29% of the features were preserved. These results indicate that iGC relied heavily (and far more than dGC) on dependencies between features for accurate classification.

S5 Recursive Feature Elimination

Two-level Recursive Feature Elimination (RFE) was implemented as described in previous studies [4][9]. First, the data were divided into N_1 (here, 10) folds. Of these, $N_1 - 1$ folds were used as "training" data, and one fold was reserved as "test" data for quantifying the generalization performance of the classifier. Training data were pooled and further divided into N_2 (here, 5) folds. The SVM classifier was then trained on $N_2 - 1$ folds (leaving out one fold) and discriminative weights were obtained. The above procedure was repeated N_2 times by leaving out each fold, in turn. Average weights were then computed by averaging the absolute values of the discriminative weights across the N_2 runs. Next, the feature (connection) contributing the lowest average weight was discarded, and the classifier was trained again with only the retained set of features. This procedure of feature selection and training was repeated until no more features remained. At this stage, the generalization performance for every set of retained features (each RFE level) was assessed using the left out "test" data. The entire procedure was repeated N_1 times by leaving out each fold of the original data, in turn, as test data. Final generalization performances and discriminative weights of each RFE level were obtained as the average over N_1 folds. We selected the set of connections at the RFE level at which the generalization performance reached an "elbow": the minimum set of connections at which generalization performance dipped dramatically from its maximal level. To identify this elbow we adopted the following procedure: The RFE curves were first smoothed using a moving average filter (length: 5 features). Then the first derivative was computed as a first order difference by subtracting adjacent values. The elbow is defined as the point where the first derivative changes from a positive value to near zero. Therefore we took the left most point at which the first derivative deviated significantly from zero. This corresponded well with our visual estimate for the case of iGC, and dGC at 1x, 3x and 5x down sampling. For the case of the RFE curve with 7x downsampling, the elbow was identified by visual inspection.

S6 Comparison with partial correlations

We compared the performance of classification based on GC measures with that based on partial correlations (PC). We observed that PC connectiviy performed consistently better than GC connectivity for classifying task from rest (Figure S5B). The better performance of PC could be due to the following reasons. First, estimators based on instantaneous correlations alone are typically less susceptible to noise than those that incorporate lagged correlations. This is due to the fact that the estimation of lagged-covariance is susceptible to errors from noise at multiple timepoints. For illustration, consider a VAR(1) generative model $\mathbf{x}(t) = A\mathbf{x}(t-1) + \mathbf{e}(t)$. The lagged covariance matrix is given by $\Sigma_1 = \mathbb{E}\left[\mathbf{x}(t)\mathbf{x}(t-1)^\top\right] = \mathbb{E}\left[\left(A\mathbf{x}(t-1) + \mathbf{e}(t)\right)\mathbf{x}(t-1)\right]^\top = A\mathbb{E}\left[\mathbf{x}(t-1)\mathbf{x}(t-1)^\top\right] + \mathbb{E}\left[\mathbf{e}(t)\mathbf{x}(t-1)^\top\right]$; the variability of the interaction-term $\mathbf{e}(t)\mathbf{x}(t-1)^\top$ contributes to the variance of Σ_1 in addition to to the variability in computing the instantaneous correlation. Second, information theoretic measures like dGC require sufficient number of samples for reliable estimates and accurate classification, as demonstrated in Figure S6.

S7 Estimation of coherence between two network time series

We used the Chronux toolbox [3] to compute the coherence between regional time series. We chose two connections that were identified exclusively at two of the downsampling rates viz language to visuospatial network (3x), and language to higher visual network (5x). After mean removal, the time series of language and resting conditions were provided as input to the *coherencyc.m* function. For each subject, we then computed the difference between coherence in the language task minus the coherence in the resting state. The plots in Fig. 5D (lower panel, main text) are obtained by taking the mean and standard error of the coherence (at each frequency) across subjects.

Supplementary Figures and Tables

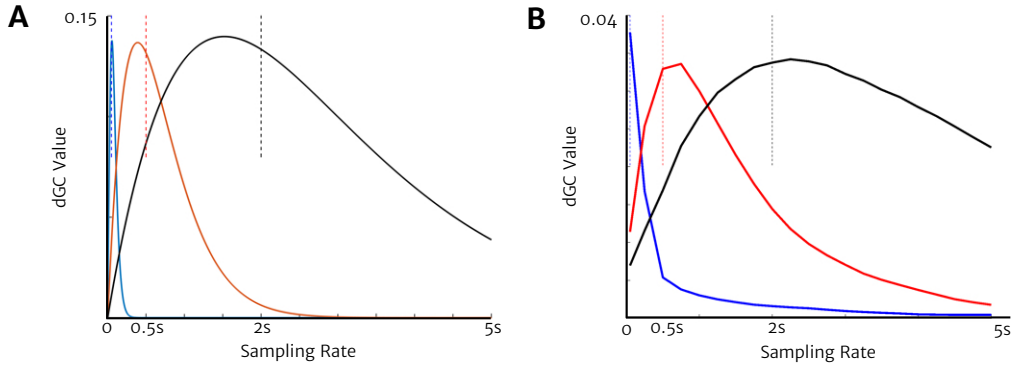

Figure S1: **Variation in dGC values at different sampling rates** : A minimal two node network with one positive connection between the nodes was used in this simulation. (A) The analytic solution of estimated dGC [2] for the connection at three different process timescales - 50 ms (blue), 500 ms(red) and 2 s (black). Note that the peak of each curve matches the process timescale (dotted line). (B) Same as in A, but when the time series were also filtered with a hemodynamic response function (average of 50 simulations). As before, peak dGC values occur close to the sampling interval.

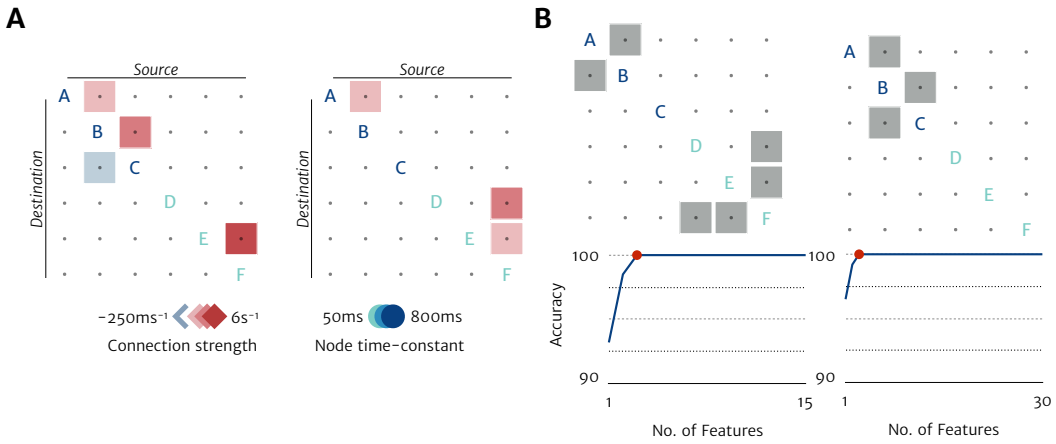

Figure S2: **Validation of Recursive Feature Elimination (RFE) using simulations**. (A) Two networks used in the simulations. The first three nodes of the networks have slow (2s) decays and last three have fast (50 ms) decays. 100 fMRI time series were simulated and sampled at a TR=2 s. (B) (Bottom) RFE analysis was done on the iGC and dGC measures estimated from the time series and the optimal number of features was identified based on the elbow point of the generalization performance curve. (Top) The optimal identified features for both iGC (left) and dGC (right) correspond closely to the connections in the "ground truth" matrix. iGC could not estimate reciprocal connections whereas dGC could not estimate connections at a timescale much faster than the sampling rate.

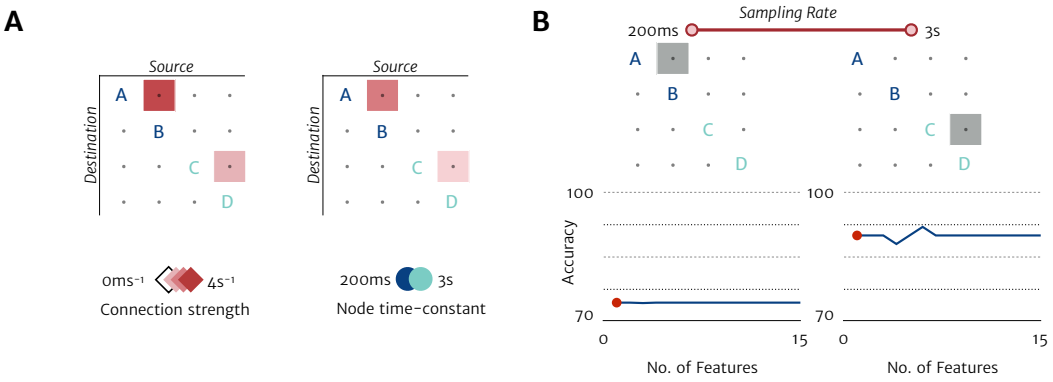

Figure S3: **Validation of RFE using simulations at different sampling rates**. (A) Two networks used in the simulations. The first two nodes of the both networks have fast (200 ms) decay while the next two nodes have slow (3s) decay. There is one fast and slow connection in each, but with different magnitudes. As before, 100 simulated fMRI time series were generated. Time series were sampled at two different sampling time periods – TR=200 ms and TR=3 s – and functional connectivity estimated with dGC. (B) In each case RFE estimated precisely one connection at a timescale corresponding to the respective TR (200 ms, left or 3 s, right). Other conventions are the same as in Figure S2B.

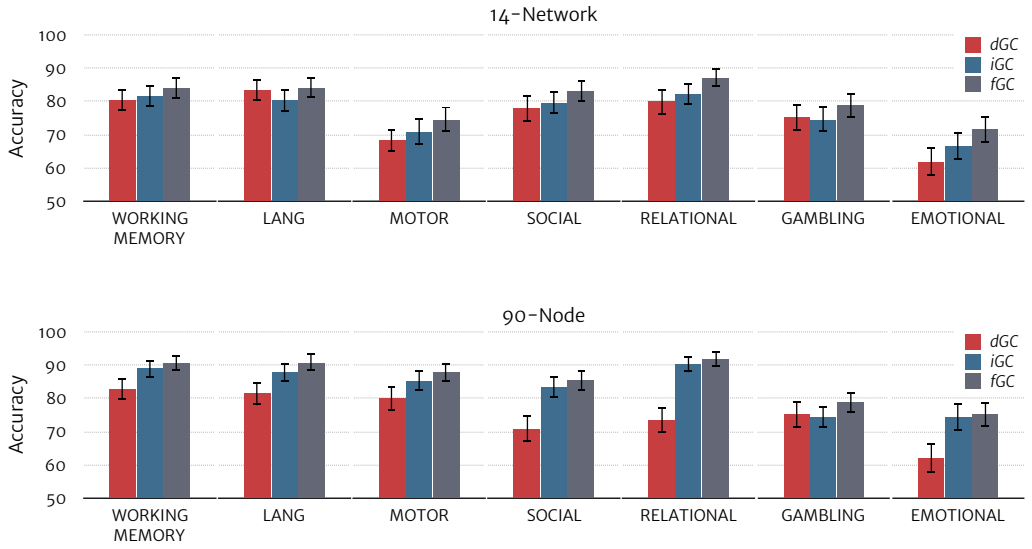

Figure S4: **Classification accuracies based on GC for task vs. rest (all tasks)** Leave-one-out classification accuracies for distinguishing seven different task-datasets from resting-state (pairwise classification). (Top) Classification accuracy with dGC, iGC and fGC networks as features, based on the 14-network parcellation. (Bottom) Same as top panel, but classification accuracies for the 90-region parcellation. Other conventions are the same as in Figure 3A, main text

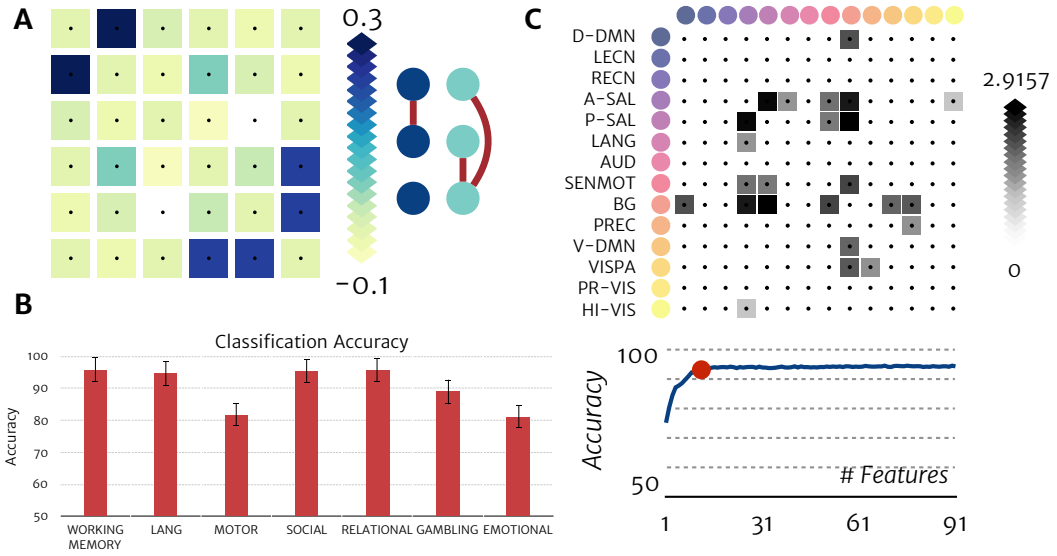

Figure S5: **Connectivity estimation with partial-correlations.** (A) The partial-correlation matrix and the reconstructed network, computed from simulated timeseries generated by Network H (Fig. 1A, main text). Conventions are the same as in Fig. 1A of main text. (B) Accuracy of classification based on PC-features, for discriminating resting state from each of the seven tasks. (C) RFE curves, with classification accuracy as a function of remaining features, for PC-based classification. Other conventions are the same as in Figure 4, main text

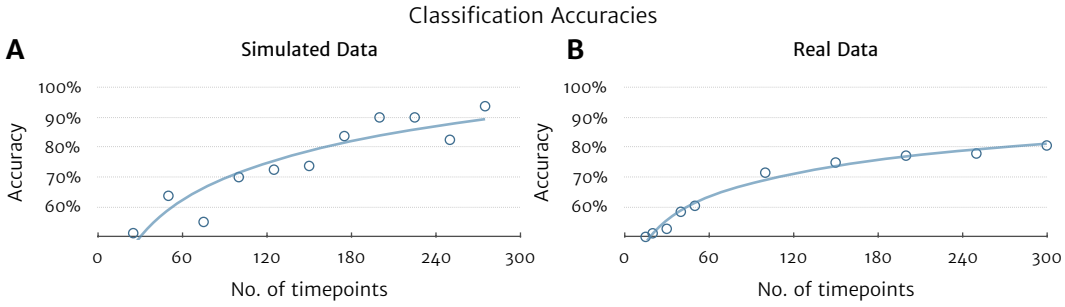

Figure S6: **Variation of classification accuracy for dGC connectivity with number of timepoints.** Classification accuracy, based on dGC, as a function of the length of the timeseries used for estimating the dGC matrix. (A) Classification accuracy for networks estimated from simulated data. Timeseries were simulated with two different "ground truth" networks (Fig. 1A-B) and used for dGC estimation. (B) Classification accuracies with increasing number of timepoints in real fMRI data, for discriminating resting state and the language task.

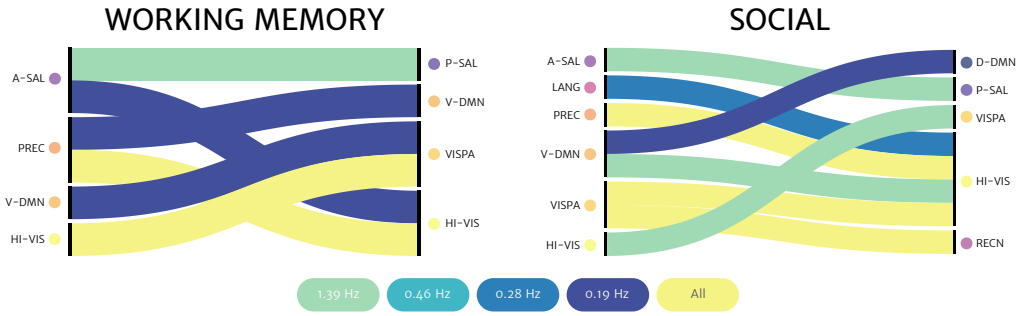

Figure S7: **Connectivity at different timescales – other tasks.** Discriminative connections identified by dGC for the (A) working memory and the (B) social tasks. Connections exclusive to different sampling-rates, and ones common to all sampling-rates are shown. Other conventions are the same as in Figure 5, main text.

Task	Description
WORKING MEMORY	A version of the n-back task, requires holding sequences in memory.
LANG	Participants listen to brief stories and in the end are asked questions about the stories.
MOTOR	Involves moving fingers, toes or tongue in response to visual cues.
SOCIAL	Participants are shown video clips of moving objects, and are asked to make judgments about social interactions among them.
GAMBLING	A guessing game where participants guess the number on a hidden card.
RELATIONAL	Participants are asked to identify similarities among objects of varying shapes and textures.
EMOTIONAL	Participants make comparisons between images of faces, and make judgments about the emotion portrayed.

Table S1: Descriptions of the seven tasks [1].

Short Name	Functional Network
A-SAL	Anterior Insula / Dorsal ACC (Anterior Salience Network)
AUD	Auditory Network
BG	Basal Ganglia Network
D-DMN	PCC / MPFC (Dorsal Default Mode Network)
LANG	Language Network
LECN	Left DLPFC / Parietal (Left Executive Control Network)
SENMOT	Sensorimotor Network
P-SAL	Posterior Insula (Posterior Salience Network)
PREC	Precuneus Network
PR-VIS	Primary Visual Network
HI-VIS	Higher Visual Network
RECN	Right DLPFC / Parietal (Right Executive Control Network)
V-DMN	Retrosplenial Cortex / Medial Temporal Lobe (Ventral Default Mode Network)
VISPA	Intraparietal Sulcus / Frontal Eye Fields (Visuospatial Network)

Table S2: 14 functional networks, along with their short names [10].

100206	130013	103414	141422	148941	154431	105923	164636	172130	177241
102008	130316	135528	141826	149236	154532	159239	164939	172332	177645
123824	130417	135730	142828	149337	154734	159340	165032	172433	178142
123925	130619	135932	143325	149539	105216	159441	165638	172534	178243
124220	130821	136227	104012	149741	154835	159744	165840	172938	178647
124422	102816	136732	144125	149842	154936	159946	106521	107321	178748
124624	130922	136833	144731	150524	155231	160123	166438	173334	178849
124826	131217	137027	144832	105014	155635	160729	166640	173435	178950
125525	131419	137128	145127	150625	155938	160830	167036	173536	108121
126325	131722	137229	145834	150726	156031	106016	167238	173637	179245
126628	131823	137633	146129	150928	156233	161327	167743	173738	179346
102311	131924	103515	146331	151223	156334	161630	168240	173839	180129
127327	132017	137936	104416	151425	156435	161731	168341	173940	180432
127630	133019	138231	146432	151526	156536	162026	168745	174437	180735
127933	103111	138534	146533	151627	105620	162228	107018	175035	180836
128026	133625	138837	146937	151728	156637	162329	169444	107422	180937
128127	133827	139233	147030	151829	157336	162733	169747	175237	181131
128632	133928	139637	147737	152831	157437	162935	169949	175338	108222
128935	134021	139839	148032	105115	157942	163129	170631	175439	181232
129028	134223	140117	148133	153025	158035	163331	170934	175742	181636
129129	134324	140319	148335	153227	158136	106319	171330	176037	182436
102513	134425	103818	148436	153429	158338	163432	100408	176239	182739
129331	134728	140824	100307	153631	158540	163836	171532	176441	183034
129634	134829	140925	104820	153833	158843	164030	171633	176542	183337
129937	135225	141119	148840	154229	159138	164131	172029	107725	185139
185341	192136	198653	204622	211316	231928	283543	310621	358144	395756
108323	192439	109830	205119	211417	233326	112314	311320	113619	395958
185442	192540	198855	205220	211720	236130	284646	316633	361234	397154
185846	192641	199453	205725	211922	237334	285345	316835	361941	397760
185947	192843	199655	110613	212015	111716	285446	317332	365343	397861
186141	193239	199958	205826	212116	239944	286650	318637	366042	406432
186444	109123	200008	206222	212217	245333	287248	112920	366446	406836
187143	194140	200109	207123	212318	246133	289555	321323	371843	412528
187345	194645	200210	207426	212419	248339	293748	322224	377451	114217
187547	194746	200311	208024	212823	249947	295146	329440	378857	414229
187850	194847	110007	208125	111413	250427	297655	330324	379657	415837
188347	195041	200614	208226	213421	250932	112516	333330	380036	422632
108525	195445	201111	208327	214019	251833	298051	334635	381038	424939
188448	195849	201414	111009	214221	255639	298455	336841	381543	429040
188549	195950	201515	209127	214423	256540	299154	339847	382242	432332
188751	196144	201818	209228	214524	101006	300618	341834	385450	433839
189349	100610	202113	209329	214726	112112	303119	346137	386250	436239
189450	109325	202719	209834	217126	257542	303624	113215	387959	436845
190031	196346	203418	209935	217429	257845	304020	346945	389357	441939
191033	196750	110411	210011	220721	263436	304727	348545	390645	101107
191336	197348	203923	210415	111514	268749	305830	352132	391748	114318
108828	197550	204016	210617	221319	268850	307127	352738	393247	114419
191841	198249	204319	211114	224022	270332	308129	353740	113922	114621
191942	198350	204420	211215	227432	275645	308331	355239	393550	114823
192035	198451	204521	111312	228434	280739	309636	356948	395251	114924

Figure S8: **HCP subject identifiers.** Unique identifiers for the 500 subjects from the HCP database [6] that were analyzed in this study.

References

[1] D. M. Barch, G. C. Burgess, M. P. Harms, S. E. Petersen, B. L. Schlaggar, M. Corbetta, M. F. Glasser, S. Curtiss, S. Dixit, C. Feldt, et al. Function in the human connectome: task-fMRI and individual differences in behavior. *NeuroImage*, 80:169–189, 2013.

[2] L. Barnett and A. K. Seth. Detectability of Granger causality for subsampled continuous-time neurophysiological processes. *Journal of Neuroscience Methods*, 275:93 – 121, 2017.

[3] H. Bokil, P. Andrews, J. E. Kulkarni, S. Mehta, and P. P. Mitra. Chronux: a platform for analyzing neural signals. *Journal of Neuroscience Methods*, 192(1):146–151, 2010.

[4] F. De Martino, G. Valente, N. Staeren, J. Ashburner, R. Goebel, and E. Formisano. Combining multivariate voxel selection and support vector machines for mapping and classification of fMRI spatial patterns. *NeuroImage*, 43(1):44–58, 2008.

[5] J. F. Geweke. Measures of conditional linear dependence and feedback between time series. *Journal of the American Statistical Association*, 79(388):907–915, 1984.

[6] M. F. Glasser, S. N. Sotiropoulos, J. A. Wilson, T. S. Coalson, B. Fischl, J. L. Andersson, J. Xu, S. Jbabdi, M. Webster, J. R. Polimeni, et al. The minimal preprocessing pipelines for the Human Connectome Project. *NeuroImage*, 80:105–124, 2013.

[7] M. Ojala and G. C. Garriga. Permutation tests for studying classifier performance. *Journal of Machine Learning Research*, 11:1833–1863, 2010.

[8] J. D. Power, A. L. Cohen, S. M. Nelson, G. S. Wig, K. A. Barnes, J. A. Church, A. C. Vogel, T. O. Laumann, F. M. Miezin, B. L. Schlaggar, et al. Functional network organization of the human brain. *Neuron*, 72(4):665–678, 2011.

[9] S. Ryali, K. Supekar, D. A. Abrams, and V. Menon. Sparse logistic regression for whole-brain classification of fMRI data. *NeuroImage*, 51(2):752–764, 2010.

[10] W. Shirer, S. Ryali, E. Rykhlevskaia, V. Menon, and M. Greicius. Decoding subject-driven cognitive states with whole-brain connectivity patterns. *Cerebral Cortex*, 22(1):158–165, 2012.